Purdue University

Purdue e-Pubs

CTRC Research Publications

Cooling Technologies Research Center

3-1-2023

The capillary length scale determines the influence of bubble-fin interactions and prediction of pool boiling from heat sinks

M. Winter

Justin Weibel
jaweibel@purdue.edu

The Capillary Length Scale Determines the Influence of Bubble-Fin Interactions and Prediction of Pool Boiling from Heat Sinks

Maureen Winter, Justin A. Weibel
Cooling Technologies Research Center
School of Mechanical Engineering
Purdue University, West Lafayette IN, USA
winter48@purdue.edu; jaweibel@purdue.edu

Heat sinks have the capability of increasing the operating heat flux limits of two-phase immersion cooling for passive electronics thermal management. For arrays of fins, investigation of the heat-flux-dependent variation of boiling regimes that can manifest along the fin height is required to predict performance and facilitate heat sink design. Existing methods for the prediction of fin boiling heat transfer which account for a variable heat transfer coefficient along the fin height assume single, isolated fins that behave like a boiling flat surface. When applied to fin arrays, thresholds for fin height and array spacing where this assumption holds true are not known. To establish when fins in an array can be described as isolated and follow flat surface boiling behavior, pool boiling experiments are performed using copper heat sinks in two fluids with vastly different properties: HFE-7100 and water. The spacing and height of the longitudinal fins are varied with respect to the capillary length scale, L_b, of both fluids, and high-speed visualizations enable the identification of different boiling regimes and bubble confinement between fins. Predictions based on the single, isolated fin assumption are compared to the experimental boiling curves. Heat transfer from heat sinks with both height and spacing above the capillary length scale is accurately predicted in both fluids. However, spacings smaller than L_b lead to bubble confinement, which causes the superheat at each heat flux to be lower than the predictions using the flat surface, particularly at low heat fluxes. Further, heights shorter than L_b are unable to support boiling along the fin sidewall once film boiling initiates at the base. This work firmly establishes the fluid capillary length as the key length scale at which these confinement and height effects need to be considered for accurate prediction and design of heat sinks for two-phase immersion cooling applications.

Keywords—immersion cooling, pool boiling, heat sinks, extended surfaces, fin arrays

I. Introduction

As the power density of electronic devices increases, so does the challenge of efficiently dissipating heat to maintain safe operating temperatures. Particularly in large-scale, power-dense electronics systems where thermal management requires a significant energy input, such as data centers, common air-cooling solutions are fast becoming inadequate and are not energy efficient [1, 2]. One promising solution for passive thermal management of next-generation electronics is two-phase immersion cooling. During boiling, the latent heat of the fluid absorbs large amounts of energy, effectively cooling the heat source while the vapor generated is passively lifted away by buoyancy. However, if too much vapor is generated at high surface heat fluxes, the formation of an insulating vapor film over the surface dramatically reduces the heat transfer rate, a condition known as critical heat flux (CHF). The dielectric fluids required for immersion cooling of electronics have a typical CHF value on the order of 10s W/cm^2 from a flat surface, insufficient for modern high-power devices that can generate 100s W/cm^2 at the source.

There are several boiling enhancement strategies available, such as those recently reviewed in Refs. [3–5]. As a general overview, one option is through microscale roughening of the surface to provide more bubble nucleation sites and thereby increased boiling heat transfer at lower superheats [6–8]. Coating the surface with microporous structures has a similar effect, enhancing nucleate

boiling heat transfer at the surface [9, 10]. Nanoscale surface coatings can also provide boiling enhancement, as reviewed in Refs. [11, 12], through effects such as increasing surface wettability to delay CHF [13] or leveraging non-wetting surface properties that increase bubble nucleation density [14]. Patterning a surface with multiple regions of contrasting wettability [15, 16] or tailoring the dynamic wetting characteristics of a surface [17] are promising boiling enhancement strategies that combine multiple different desired wettability characteristics. While there are important challenges for the implementation of two-phase cooling in data centers, such as fluid-material compatibility and leakage issues [1], an overall concern associated with enhancement techniques that rely on coatings and surface properties is their long-term reliability.

Finned boiling surfaces (i.e., heat sinks) provide a reliable solution by increasing the boiling surface area, thereby effectively decreasing the surface heat fluxes. However, even in the case of constant cross section fin arrays, determining optimized fin height and array spacing under conditions of pool boiling is a challenge, as is further discussed in the sections that follow. This study seeks to determine the required conditions for accurate performance predictions to provides guidelines for designing heat sinks specifically for boiling.

A. Prediction of pool boiling from fins

Because the temperature varies along the height of a fin, it is possible for multiple different boiling regimes to occur along extended surfaces depending on the local surface superheat. In particular, the lower superheat at the top of the fin means that these tips can operate in a nucleate boiling regime even while the higher superheat at the base causes film boiling [8, 18–21]. Under these conditions, efficient nucleate boiling along the sides of the fin prevents temperature runaway and CHF. Predicting the boiling heat transfer from extended surfaces where multiple boiling regimes are sustained is a challenge, even when considering single fins of a simple geometry. The most accepted prediction method was originally proposed and developed by Haley and Westwater [22], from the analysis of a single fin, and then later used in various later studies [18, 20, 23, 24]. This method assumes that the boiling heat transfer coefficient, h, as a function of the surface superheat, ΔT_b, on a flat surface describes the boiling performance along the entire fin surface, regardless of fin shape or orientation. Once this function $h(\Delta T_b)$ is predicted or measured separately for a flat surface, a standard fin analysis incorporating the variable heat transfer coefficient along the fin can be performed. While other predictive methods for boiling heat transfer from fins exist [8, 19, 25], all similarly use an analysis that assumes single, isolated fins.

B. Effects of fin height and array spacing in heat sinks

In the case of a heat sink having an array of multiple fins, close spacing between comparably tall fins in the array can lead to confinement of vapor bubbles during their growth and departure. This further complicates the prediction of boiling performance and challenges the assumption that the fins are single and isolated and that the flat surface $h(\Delta T_b)$ can be used to describe boiling along the sides of fins. Both fin height and array spacing can affect the boiling behavior, and must be considered when applying the assumption.

Fin height has been observed to primarily affect boiling performance at high heat fluxes of operation, with taller fins able to dissipate higher heat fluxes than shorter fins at a given base superheat [8, 23, 26]. Fantozzi et al. [25] noticed that their predictions of fin heat transfer performance were more accurate for longer fins, while others [8, 26] have observed that overly tall fins lead to vapor confinement issues that could hamper the ability to predict performance. However, no specific recommendations or guidelines were offered on the height range over which predictions were accurate. Fin array spacing generally affects boiling performance at lower heat fluxes, with smaller spacing leading to lower superheats (improved performance compared to larger spacings) at each heat flux [24, 26]. Based on visualizations, small spacing combined with tall fins can lead to vapor buildup at the base of the fins and

confinement that changes boiling performance [26]. The threshold spacing at which fins act independently has not been established in these past studies, and in instances where guidance is offered [27], it is not generally applicable across different heat sink designs.

The overall effects of fin height and array spacing are well summarized in the experiments of Yu and Lu [26], who boiled FC-72 on pin fin heat sinks varying both height and spacing. All fins with the largest spacing of 2 mm and heights longer than 0.5 mm had boiling curves that overlapped until high heat fluxes, where the tallest 4 mm fins were able to extend to the highest CHF. However, when spacing was decreased from 2 mm to 0.5 mm, the shortest fins had the lowest base superheat compared all others at low heat fluxes, clearly indicating the interdependent influence of fin height and spacing. Similar interdependence was also reported for boiling refrigerants and water at pressures lower than atmospheric [18, 28].

There have been a few studies describing boiling from fins with additional micro-scale boiling enhancement features [8, 23, 29]. Of particular interest is the work of Mudawar and Anderson [23] that demonstrated the $h(\Delta T_b)$ boiling behavior of a flat surface enhanced with microfin studs could be used to predict the performance of similarly studded fins, following the prediction approach of Haley and Westwater [22]. While exploration of enhanced fins is of interest, a deeper understanding of boiling on smooth finned structures is still required and can inform such enhancement strategies.

C. Scope and hypothesis

It is necessary to have accurate methods to predict boiling from arrays of fins to allow for the design of heat sinks for two-phase immersion cooling. In particular, the above sections revealed that existing prediction methods rely on the assumptions of single, isolated fins and the temperature-dependent sidewall heat transfer coefficient $h(\Delta T_b)$ taken from a flat surface. However, there is a need to determine the fin height and array spacing at which these assumptions hold true, as past boiling experiments on heat sinks indicate significant deviations from these assumptions.

An exhaustive collection of observations from the literature for pool boiling from single fins and arrays of fins is compiled in Table 1. Based on the spacing and height effects observed, absolute fin dimensions, and working fluids used, we hypothesize that the capillary length of the fluid is a general measure that determines the threshold fin height and array spacing at which fins can be treated as independent. The capillary length scale is defined as

$$L_b = \sqrt{\frac{\sigma}{g(\rho_l - \rho_v)}} \tag{1}$$

where σ is the surface tension of the fluid, g is the acceleration due to gravity, and ρ_l and ρ_v are the liquid and vapor densities of the fluid, respectively, with all properties taken at the saturation condition. While the capillary length scale has been used to define the onset of confinement effects under flow boiling conditions [30], the use of the capillary length scale for determining the critical lengths of pool boiling heat sink dimensions has not be considered. It is generally expected that if both height and spacing are larger than L_b, fins in an array can be described as isolated and will follow the flat surface $h(\Delta T_b)$ boiling behavior. However, if either the height or spacing is below L_b, and the vapor bubble sizes become much larger than these heat sink dimensions, then bubble-fin interactions will change the boiling behavior.

Table 1: Observations in the literature on prediction methods as wells as effects from fin height and array spacing.

Reference	Working Fluid	Material	Cross Section, Profile	Observations
Single Fins:				
Haley and Westwater (1966) [22]	Isopropyl R-113	Copper	Circular, Rectangular Circular, Turnip shaped	Accurate predictions using $h(\Delta T_b)$ from a flat surface for the cylindrical fins up to CHF
Cash et al. (1971) [20]	R-113	Copper	Circular, Double triangular	Successful predictions using $h(\Delta T_b)$ from the flat surface, with accuracy dependent on fin attachment
Lai and Hsu (1967) [19]	Water Freon Isopropyl	Aluminum	Longitudinal, Rectangular	Less accurate predictions using average h values for each regime with regime length iteratively solved
Fantozzi et al. (2000) [25]	HCFC141b	Aluminum	Longitudinal, Rectangular	1D assumption confirmed using average h values determined from thermocouples embedded in the fin
Mudawar and Anderson (1993) [23]	FC-87	Copper	Circular, Rectangular	Low heat fluxes, varying fin lengths have similar performance; high heat fluxes, taller fins lower superheats
Fin Arrays:				
Rainey and You (2000) [8]	FC-72	Copper	Square, Rectangular	Tall fins did not have accurate CHF predictions. All heights have similar performance until CHF
Mudawar and Anderson (1993) [23]	FC-87 FC-72	Copper	Circular, Rectangular	Predictions using $h(\Delta T_b)$ from a flat surface were accurate, though trends were better captured for the array with larger spacing
Guglielmini et al. (1996) [24]	Galden HT55	Copper	Square, Rectangular	Hypothesized that close fin spacing caused boiling to be less efficient even if had higher CHF
Klein and Westwater (1971) [27]	R-113 Water	Copper	Circular, Rectangular	Attempts to find minimum spacing for vapor entrapment were not generally applicable
Yu and Lu (2007) [26]	FC-72	Copper	Square, Rectangular	Smallest spacing had lower superheats at low heat fluxes; heights larger than 0.5 mm perform similarly until high heat fluxes near CHF
McGillis et al. (1991) [28]	Water (9 kPa)	Copper	Square, Rectangular	Smallest spacings led to lowered superheats; fins with larger height and spacing had similar performance
Abuaf et al. (1985) [18]	R-113 (4-101 kPa)	Copper	Square, Rectangular	Predictions using $h(\Delta T_b)$ from a flat surface were fairly accurate for pressures near atmospheric

II. EXPERIMENTAL METHODS

In order to test the hypothesis, heat sinks are tested under pool boiling of HFE-7100 and water using the experimental facility shown in Fig. 1. These two fluids were chosen for their vastly different fluid properties, particularly those properties that determine the capillary length, L_b: ~1.0 mm for HFE-7100 and ~2.5 mm for water. The chamber and flow loop were first designed for experiments reported in [31], then subsequently modified for pool boiling experiments and used in Refs. [32–34], before being further modified for the current tests. A summary of the test facility construction, the test procedures, and a description of the test samples is provided in the subsections below.

A. Facility Description

The fluid is pumped with a gear pump at a low flow rate (~350 mL/min) from a reservoir into the boiling chamber, shown in Fig.

1, made of polyether ether ketone (PEEK) walls with polycarbonate windows for visualization. At the inlet to the chamber, flow is evenly distributed into a polycarbonate plenum that has a solid plate mounted a short distance (3.17 mm) from the bottom, such that the radial outflow through the opening at a small velocity does not interfere with the boiling on the surface below within its effectively quiescent surroundings. The boiling chamber outlet returns to the reservoir, which contains Graham condensers open to the ambient that condense all vapor generated in the chamber. Cartridge heaters in the reservoir are used for the pre-test degassing and continuously boil the fluid during the experiment to maintain saturated conditions in the reservoir. A liquid-to-air heat exchanger is placed at the outlet of the reservoir to slightly subcool the saturated liquid drawn to the pump to avoid cavitation. Saturated conditions are maintained in the chamber by boiling from the sample and supplemented as needed with immersion heaters mounted from the top wall of the chamber. A T-type thermocouple and pressure transducer are used to ensure that the chamber stays at the saturation temperature at atmospheric pressure throughout the experiments. The flow rate into the test chamber is measured using a Coriolis flow meter and controlled using a needle valve and flow bypass. Pool boiling tests were performed at multiple flow rates with both fluids to confirm that flow rate had no effect on the pool boiling performance, confirm quiescent flow conditions over the sample and demonstrate the repeatability of the experiments (see Supporting Information Figure S1).
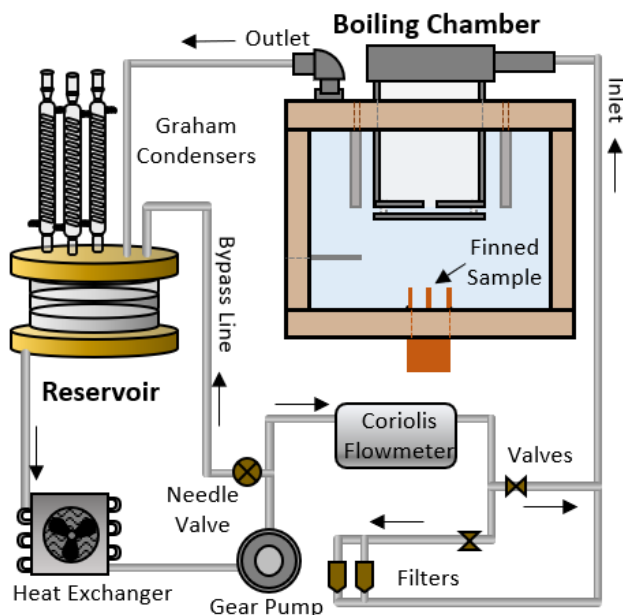

Fig. 1: Experimental facility. The flow loop is open to ambient and kept in saturation conditions by heaters in the reservoir and boiling chamber. The low flow rate and deflector plate in the boiling chamber keep the fluid above the finned heat sink quiescent during pool boiling.

All finned heat sink samples are additively manufactured from copper (Markforged Metalx™) and have a 20 mm × 20 mm base footprint area. This additive manufacturing process is chosen as it allows for fabrication of tall, thin fins that would be extremely difficult to produce in copper using traditional machining processes. The as-fabricated samples have a periodic surface roughness from the printed strands with a peak-to-valley distance of ~60 μm. The fins are longitudinal with rectangular profile, with characteristic height (H) and spacing (S) dimensions as shown in Fig. 2(b). A flat surface without fins was also fabricated using the same additive process and tested as a baseline. All samples were cleaned prior to testing to remove any oils from handling during

printing. Cleaning was performed in an ultrasonic cleaner using acetone and then isopropanol for 5 min each, followed by thorough rinsing in deionized water.

The samples are inserted into a base holder, shown in Fig. 2(a), sealed flush with a self-leveling adhesive (Dow Q3-6611), and fitted into the bottom wall of the chamber. To heat the samples, twelve ¼" diameter cartridge heaters are embedded with even spacing into the bottom of the copper samples and connected to a variable power source. Three vertical thermocouple rakes are located along the front, middle, and back of the sample, with ice-point-referenced T-type thermocouples inserted. The temperature gradients measured with these rakes are used to determine the area-averaged heat flux and extrapolated base surface temperature (at the base of the fins) assuming one-dimensional heat flow in the sample and the nominal thermal conductivity of 350 W/mK per the manufacturer datasheet. An uncertainty analysis was conducted by approximating the error in the copper block temperature gradient using the methods in [35] and the stated accuracy of the thermocouples (±1 K or 0.75% of the thermocouple reading, whichever is greater). The uncertainty in the area-averaged surface temperature is < 2.5 K for both water and HFE-7100 at all input powers. Uncertainty in the calculated heat fluxes was always <15% except at the extreme lowest input powers.

B. Test Procedure

Before each experiment, the fluid was degassed by vigorous boiling in the reservoir and from the sample for at least 2 hr with fluid flowing through the 15 um filtering subloop. The sample was then allowed to cool before starting the experiment. For each experiment, power to the sample was increased in steps of ~10-24 W for HFE-7100 and ~100-150 W for water, and then the system was allowed to reach steady state (a change in surface temperature of < 1 K/hr). Steady state data at each power were recorded for 2 min at 0.5 Hz and then averaged. For some samples at high heat fluxes, typically in regimes with dryout at the base of the fins and nucleate boiling along the sides, it became evident that the steady state criterion was overly strict and was not reached after a long time (>2 hr). In these instances, data were instead recorded after waiting up to a maximum of 45 min for the temperatures to stabilize. Tests were generally stopped when CHF was reached, as indicated by a rapid temperature increase and vapor covering the entire heat sink, such as shown in Fig. 2(c). In the case of water, many tests had to be stopped when the surface superheat exceeded 50 K, due to the higher boiling point of water and temperature limits of materials used in the construction of the base sample holder. All data were supplemented with high-speed visualization (VEO710L; Phantom Vision Research).
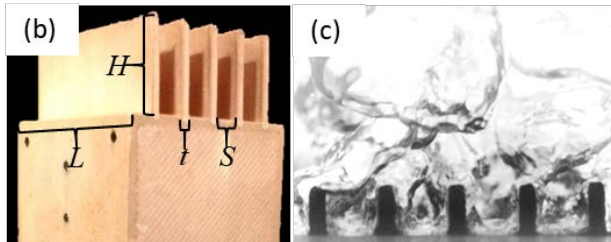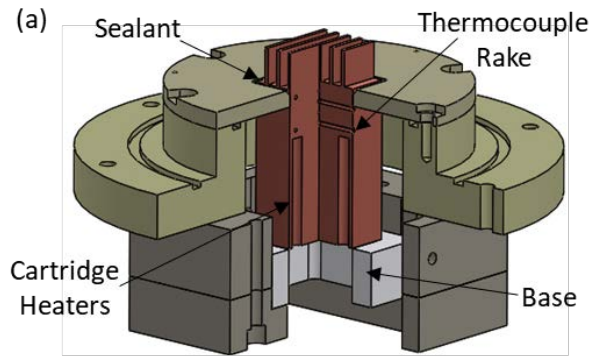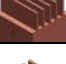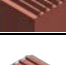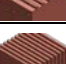
Fig. 2: (a) Sample holder showing heating and measurement elements; (b) sample with key dimensions labelled; and (c) example of CHF condition showing the vapor layer covering the entire boiling surface.
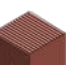
C. Test Matrix

Table 2 shows the test matrix of samples developed based on the capillary length scales of water and HFE-7100 as given by Equation (1). All samples have a constant fin thickness (t) of 1 mm and different fin heights (H) and spacings (S) of either 1.0 mm, 2.5 mm, or 8.5 mm. A single sample with 0.5 mm tall and 0.5 mm spaced fins was tested in HFE-7100 to examine what occurs when both height and spacing are below the capillary length for this fluid. The dimensions are intentionally lesser than, similar to, and larger than the capillary length scale of at least one fluid, with the specific values chosen to yield 3, 5, 10, or 13 evenly spaced fins along the 20 mm edge length of the boiling surface. Longitudinal fins were chosen to allow clear videos of the bubble-fin interactions.

Table 2: Test Matrix. All samples are tested in HFE-7100 (L_b ratio listed is for HFE-7100), while samples marked with an asterisk* are additionally tested in water.

Sample (Height-Spacing)		Parameter		
		Total Boiling Area to Footprint Ratio	H/L_b Ratio	S/L_b Ratio
H8.5-S8.5*		3.55	8.5	8.5
H2.5-S8.5*		1.75	2.5	8.5
H1.0-S8.5*		1.30	1.0	8.5
H8.5-S2.5*		5.25	8.5	2.5
H2.5-S2.5*		2.25	2.5	2.5
H1.0-S2.5		1.50	1.0	2.5
H8.5-S1.0*		9.50	8.5	1.0
H2.5-S1.0		3.50	2.5	1.0
H1.0-S1.0*		2.00	1.0	1.0
H0.5-S0.5		1.65	0.5	0.5

III. Modeling Approach

In order to identify the key length scale at which the fins in an array can be described as isolated and follow flat surface boiling behavior, a model was developed following the single-fin analysis of Haley and Westwater [22]. To incorporate a variable heat transfer coefficient, the $h(\Delta T_b)$ function was determined from the baseline flat surface and assumed to dictate the boiling behavior on the base area, fin sides, and fin tips in the heat sinks.

Established correlations calibrated to experiments using the flat surface were used to determine the heat transfer coefficient in each boiling regime. The nucleate boiling regime was determined by fitting the following power law correlation to experimental data obtained using the flat, additively manufactured surface:

$$h_{NB} = C\Delta T_b^n \tag{2}$$

where C and n are constants fitted individually for each fluid. The experimentally measured boiling curves and correlation fits for both fluids are given in see Supporting Information Figure S2. The maximum superheat for this nucleate regime, when applied to the heat sink predictions, was defined as the superheat when Equation (2) reached the heat transfer coefficient measured at CHF for the flat surface.

The natural convection regime was determined using Nusselt number correlations for a horizontal plate [36] with the superheat range from zero up to a ΔT_b that resulted in the natural convection correlation intersecting with the nucleate boiling correlation. For the film boiling regimes, the lowest superheat was determined by the intersection of two separate flat plate film boiling correlations [37, 38] while the $h(\Delta T_b)$ values of this regime were determined using [38]. For the range of superheats between nucleate boiling and film boiling, the transitional boiling regime was assumed to be a straight line connecting between the maximum nucleate boiling heat transfer coefficient with the lowest superheat of the film boiling regime, following the approach in [18]. Plots showing the piecewise $h(\Delta T_b)$ function, delineated by each regime, are shown for both working fluids in see Supporting Information Figure S3.

With the $h(\Delta T_b)$ function defined, each fin can be discretized into small volumes in one dimension along its length and energy balance equations can be applied to each segment, following a standard fin analysis with a temperature-dependent heat transfer coefficient. The boundary conditions were a specified superheat at the fin base and convection from the fin tip area. Starting from a uniform initial temperature profile, the final temperature distribution along the fin can be iteratively solved to numerically determine ΔT_b at each segment. The total heat flux dissipated through the heat sink at this base superheat is then determined by assuming all fins have the same boiling performance.

$$q''_{tot} = \frac{q_{fin}N_{fin} + h(\Delta T_b)\Delta T_b A_{space}N_{space}}{A_{base}} \tag{3}$$

where q_{fin} is the total heat dissipated by a single fin, ΔT_b is the superheat at the base of the fins, N_{fin} is the number of fins, N_{space} is the number of spaces between fins, A_{space} is the base area of the spaces between fins, and A_{base} is the base footprint of the sample, 20×20 mm^2. The resulting q''_{tot} yields a prediction of the boiling curves for various input heat sink dimensions and base superheats. By comparing these predictions with the experimental boiling curve results for finned heat sinks, any deviations can then reveal and establish the height and spacing requirements for an accurate assumption of single, isolated fins.

IV. EXPERIMENTAL RESULTS

For all boiling curve results to be discussed with HFE-7100 and water, the horizontal axis is the superheat, ΔT_b, at the base of the fins and the vertical axis is the heat flux, q'', through the base area of the sample, 20×20 mm^2. Different symbols are used to indicate the different boiling regimes that were observed to occur at the base of the heat sink between the fins: diamonds indicate uniform nucleate boiling, circles indicate partial film boiling, and triangles indicate a stable film that covers the base and connects between the fins. These regimes are determined qualitatively from the high-speed visualizations. Open symbols are used for data recorded after the steady state criterion was reached and closed symbols for data recorded after a fixed time interval, as discussed in the test procedure. Lastly, a right-pointing arrow at the end of the curve indicates when the test was ceased due to a CHF temperature excursion (no arrow is shown when the test was stopped due to reaching a superheat limit).

Selected cases from the full test matrix in Table 2 are included in the sections below to individually parse the effects of height and spacing, fixing one far above the capillary length while the other is varied. For completeness, boiling curves for all other test cases are provided in Supporting Information Figure S4.

A. Fin Height Effects

In Fig. 3(a), HFE-7100 boiling curves from three samples with varying height (1.0 mm, 2.5 mm, or 8 mm) and a constant spacing of 2.5 mm are shown in comparison to the flat surface. This spacing is over twice the capillary length of HFE-7100. When the height

is 2.5 mm and 8.5 mm, there is almost no difference in the surface superheat compared to the flat surface at low heat fluxes. Both samples overlap the boiling curve of the flat surface until it reaches CHF, after which the 2.5 mm and 8.5 mm samples are able to extend the boiling curve to higher CHF. The shortest 1.0 mm tall fins have slightly higher superheats along the entire flat surface boiling curve and CHF is also approximately the same, indicating no enhancement to the flat surface despite a 50% increase in boiling area.

The boiling curves for water in Fig. 3(b) show three samples with varying height (1.0 mm, 2.5 mm, or 8 mm) at a constant spacing of 8.5 mm, over three times the capillary length. All three fin heights have superheats that match the flat surface baseline at low heat fluxes, confirming the observation in HFE-7100 that the height of fins only effects boiling behavior at heat fluxes above the flat surface CHF. The 2.5 mm and 8.5 mm tall fins extend past the CHF of the flat surface and overlap each other up to the 50 K superheat testing limit. The 1.0 mm tall fins, shorter than the capillary length, reach CHF near the same heat flux as the flat surface, indicating they are too short to extend the boiling curve, similar to the observations in HFE-7100.

The flow visualizations shown in Fig. 4 provide insight on why the shortest fins are unable to extend the boiling curves in both fluids. The heat fluxes were chosen as the lowest observed heat flux where there is a stable film spanning the base between the fins. Key features from each sample are highlighted in the sketch made from the still image above. For HFE-7100 in Fig. 4(a), the shortest 1.0 mm tall fins cannot sustain nucleate boiling on the fins once the base area transitions to a film boiling condition; the vapor film over the base completely envelops the fins and leads to CHF at approximately the same heat flux as the flat surface. For the 2.5 mm and 8.5 mm tall fins, there is dense nucleate boiling along the sides and tips of the fins even when there is a stable film layer at the base of the fins. This efficient nucleate boiling allows the boiling curves to be extended above the CHF of the flat and indicates why the tallest fins have the best boiling performance after such a film layer develops.

As indicated in Fig. 4(b), water has much larger bubbles than HFE-7100 owing to its larger capillary length. For the 1.0 mm tall fins that are shorter than L_b for water, the CHF condition is reached when a stable film layer forms over the base and envelops the fins. Both the 2.5 mm and 8.5 mm tall fins do not reach critical heat flux when a vapor film layer forms over the base, thereby extending the pool boiling curves to higher heat fluxes. However, the 2.5 mm tall fins at the capillary length appear to be nearly fully enveloped by the film. Due to differing fluid properties, nucleate boiling is not observed along the entire fin sidewalls for these taller fins in water. Rather bubble nucleation occurs near the base of the fins, just above the vapor film, and efficient heat transfer is presumably maintained as the bubbles rise along the fin sides. The video visualizations of Fig. 4 are provided as Supporting Information.
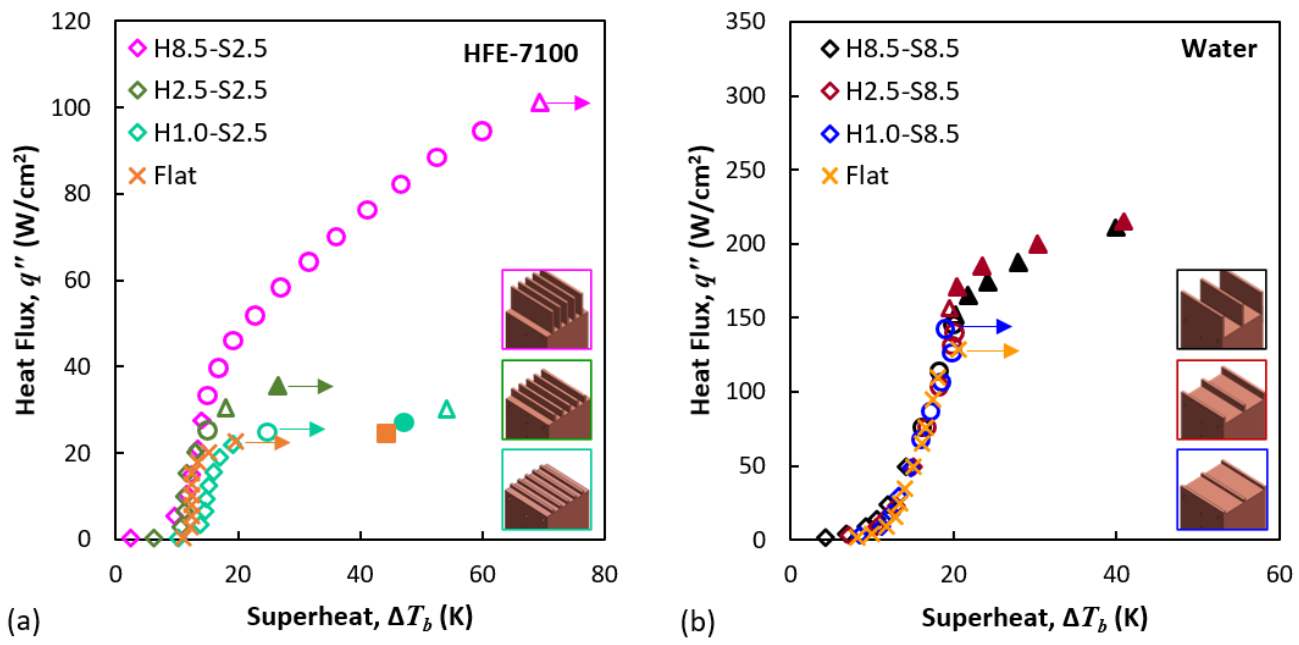
Fig. 3: Effects of fin height. (a) HFE-7100 with a constant fin spacing 2.5 × L_b (b) Water with a constant fin spacing of 3.4 × L_b. All experiments are compared with the flat surface boiling performance.
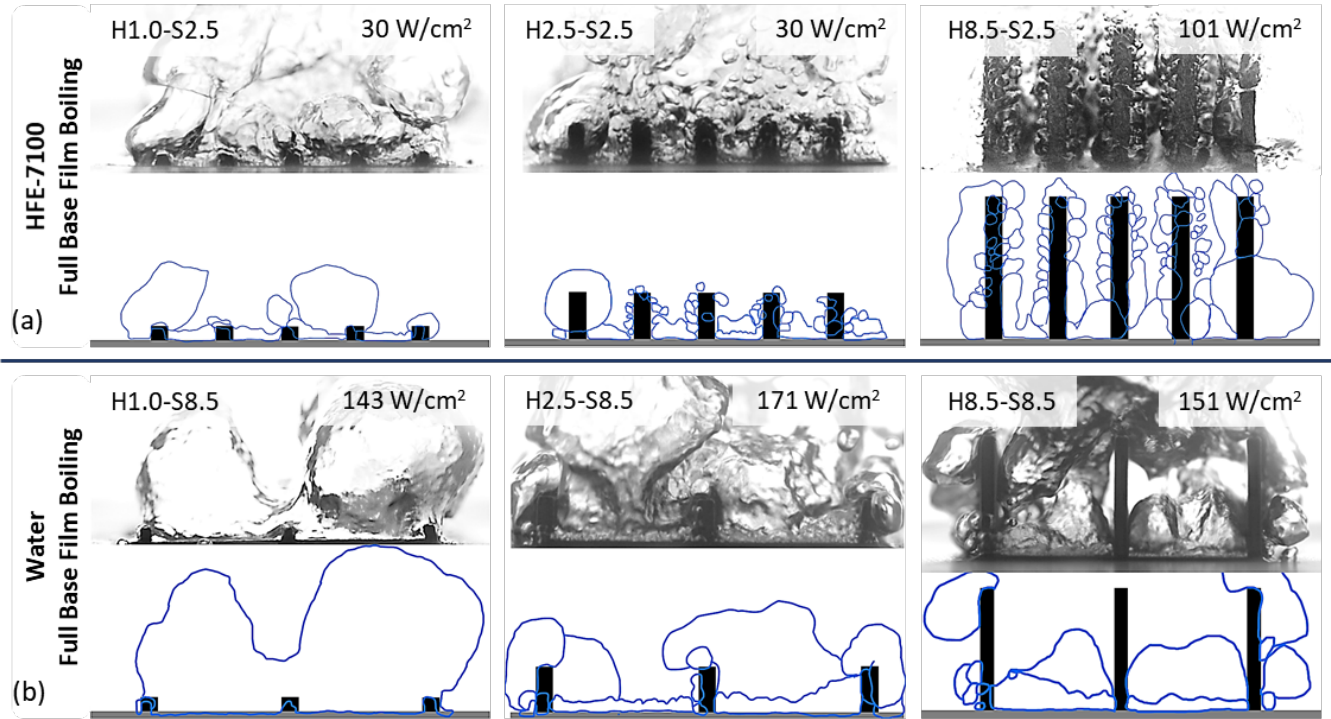

Fig. 4: Visualizations of height effects in (a) HFE-7100 and (b) water. All images were taken at the lowest heat flux where a stable film was observed to span the space between fins. The sketch below the images highlights the key aspects of the boiling condition.

B. Fin Spacing Effects

The effect of fin spacing on boiling in HFE-7100 are shown in Fig. 5(a). The fin height is held constant at the largest value of 8.5 mm while spacing is varied (1.0 mm, 2.5 mm, or 8 mm). For the larger two spacings of 2.5 mm and 8.5 mm, the boiling curves overlap at low heat fluxes throughout the nucleate boiling regime of the flat surface. Once partial film boiling begins over the base, above the CHF of the flat surface, higher heat fluxes are dissipated for the 2.5 mm spacing than 8.5 mm at each superheat, a result of the larger number of fins. The boiling behavior changes for fins spaced most closely at 1.0 mm. The superheat at each heat flux is lower for the entire boiling curve, indicating that the confinement of vapor between the 1.0 mm spacing fins has some effect on the performance. It is also clear that as spacing decreases for these tall fins, a stable vapor film does not develop over the base surface (indicated by the triangular symbols) until higher heat fluxes.

For boiling on the same heat sinks in water, with the results shown in Fig. 5(b), the general effects of fin spacing are quite similar to HFE-7100. Again, for the 2.5 mm and 8.5 mm spacing, the boiling curves overlap the flat surface boiling curve up to its CHF, above which the larger number of fins for the 2.5 mm spacing achieves higher heat fluxes at each superheat versus the 8.5 mm spacing. At the smallest spacing of 1.0 mm, below the capillary length, the superheat is lower at each heat flux, resulting in a more linear boiling curve. For spacings smaller than 8.5 mm, the formation of a stable vapor film over the base is increased to heat fluxes significantly above the CHF of the flat surface.

The flow visualizations show clear confinement of the vapor bubbles between fins when the spacing is at or below the capillary length scale of each fluid. In Fig. 6(a) showing HFE-7100 boiling at heat fluxes slightly above the CHF of the flat surface, once the spacing is reduced to 1.0 mm (near the capillary length), the bubbles no longer have uniform nucleation across the entire surface. Instead, individual bubbles span the entire gap between the fins, as indicated in the still image and the sketch below. The flow visualizations for boiling from the same heat sinks in water are shown in Fig. 6(b). Even at heat fluxes below the CHF of the flat surface, at 2.5 mm spacing, the bubbles begin to fill the entire space between fins, and for 1.0 mm spacing, below the capillary length, the vapor is extremely confined and billows out in front of the fins. The video visualizations of Fig. 6 are provided as Supporting Information.
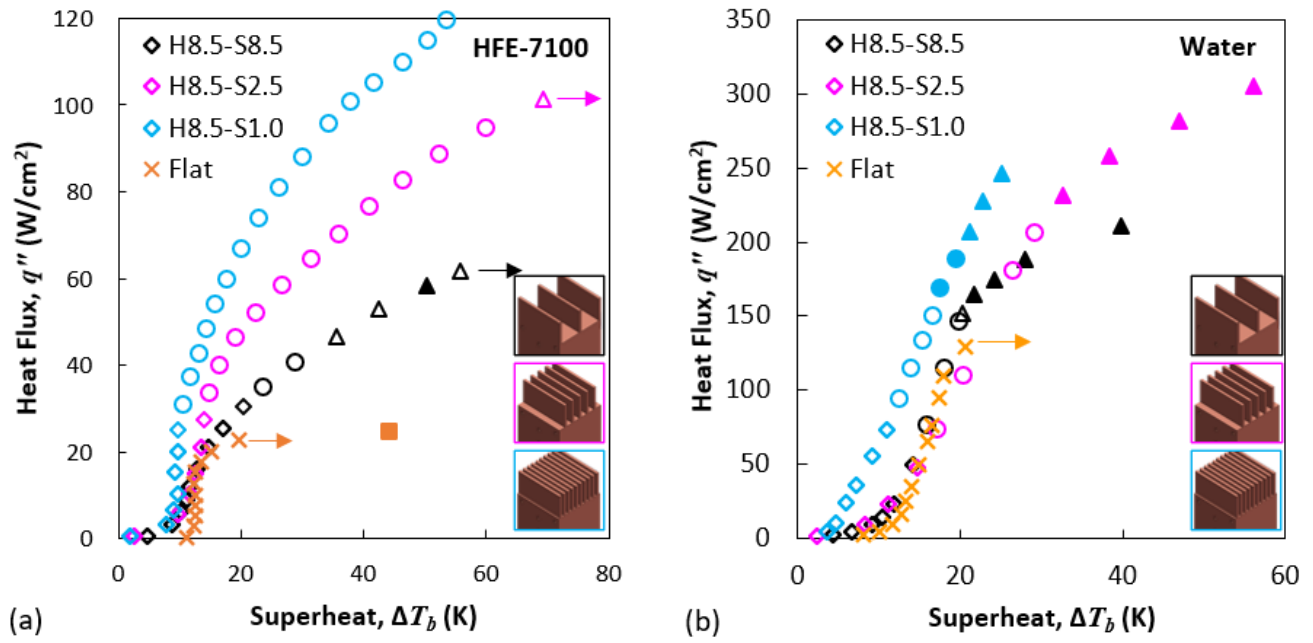
Fig. 5: Effects of fin spacing. (a) HFE-7100 at a constant fin height of $8.5 \times L_b$ (b) Water at a constant fin height of $3.4 \times L_b$. All experiments are compared with the flat surface boiling performance.
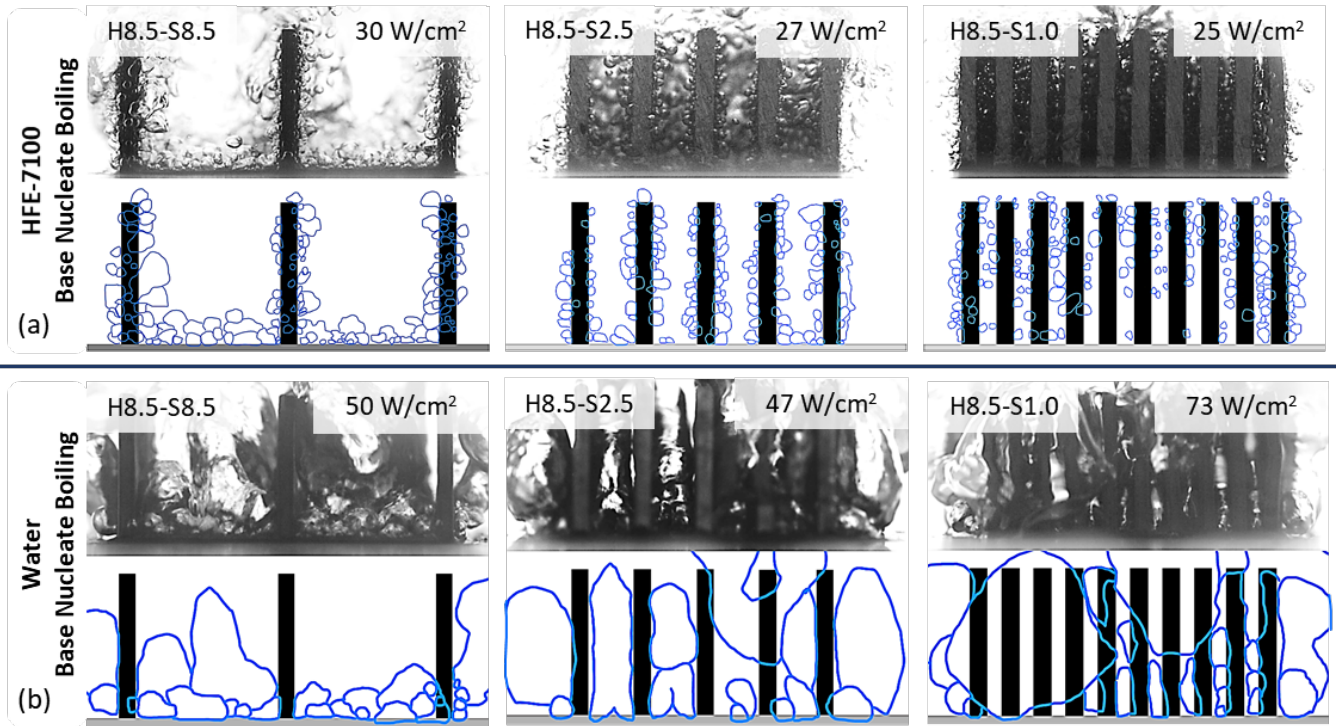

Fig. 6: Visualizations of spacing effects for (a) HFE-7100 and (b) water. All images were taken at the highest heat flux where essentially uniform nucleate boiling was observed across the boiling surface. The sketch below the images highlights the key aspects of the boiling condition.

Model predictions are compared with experimental data to identify the fin height and array spacing length scales at which the fins behave independently as assumed. Two examples of boiling curve predictions are given with the experimental data in Fig. 7. For sample H2.5-S8.5 in HFE-7100, where both height and spacing are well above the capillary length, the prediction line overlays the experimental data. The boiling regime changes are visible in the prediction line through changes in the line slope. The prediction has a steep increase in slope at the transition from natural convection to nucleate boiling, while the slope sharply decreases when there is a transition to film boiling predicted over the base area, and then slowly asymptotes to horizontal while closely following the experimental data. The predicted CHF is defined as when the predicted heat flux was no longer increasing with superheat (i.e., is horizontal), and accurately matches the experimental CHF. Sample H1.0-S2.5, on the other hand, shows a case where the prediction/experiment agreement is not as ideal. The 1.0 mm fin height is on the same order as the capillary length, and the entire prediction curve shows a lower superheat at each heat flux. Of key importance is the CHF value, since the prediction indicates ~15% increase in CHF compared to the experimental data, indicating that the shorter fins are unable to sustain a predicted stable film at the base.
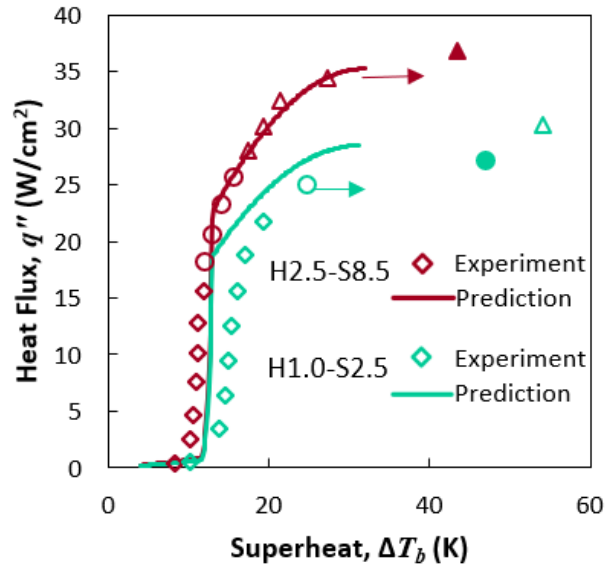

Fig. 7: Experimental and predicted boiling curves for samples in HFE-7100. H2.5-S8.5 has both fin height and spacing well above L_b and excellent prediction agreement. H1.0-S2.5 has only fin spacing above L_b, resulting in an over-predicted CHF.

While Fig. 7 provides a clear one-to-one comparison for individual boiling curves, the plots become overly cluttered when comparing predictions and experimental data across many different boiling curves. Therefore, in the subsection that follows, plots of the predicted (vertical axis) versus measured (horizontal axis) superheat ΔT_b values are shown. The solid black lines at 45 degrees therefore indicate an exact match, with dashed lines indicating $\pm15\%$ error bounds. The symbols follow the same style as in the boiling curves; note that no CHF information is portrayed on these plots.

A. Superheat

Comparisons of the predicted and measured boiling superheats for all samples tested in HFE-7100 are given in Fig. 8, where each panel groups together samples based on whether the fin height and/or spacing are below, at, or above the capillary length. In Fig.

8(a), all samples with both height and spacing greater than L_b are shown. There is good prediction agreement with the experiments, mostly within 15% for 2.5 mm tall fins. For the 8.5 mm tall samples, there is worse agreement between the predictions and the experiments at high heat fluxes. However, the predictions are parallel to the 45 degree line, indicating that the boiling behavior is captured by the model but with some constant offset, even though the height of the fins is over eight times L_b. Fig. 8(b) shows cases where the fin spacing is larger than L_b, but their height is at the capillary length scale. For these samples, the agreement is good, but with one outlying datapoint indicating that decreasing spacing may leads to less accurate predictions.

Reductions in the fin spacing to or below the capillary length causes more drastic disagreement between the predictions and experiments in HFE-7100. In Fig. 8(c), samples with height larger than L_b and spacing at the capillary length are shown. It is clear that the overall boiling behavior is not well captured by the predictions that assume isolated fin boiling. As the superheat increases, the experimental values are increasingly underpredicted, indicating that confinement plays a significant role and is changing the boiling performance from the fin sidewalls on these samples as compared to the heat transfer coefficient imposed in the model based on a flat surface. Fig. 8(d) shows samples having both fin height and spacing at or below the capillary length. For sample H1.0-S1.0, there is reasonable agreement at low superheats; however, when both spacing and height are below the capillary length, for sample H0.5-S0.5, the predictions do not accurately capture any portion boiling behavior. For further comparison, the boiling curve predictions overlaid on the experimental data for all samples compared in Fig. 8 are given as Supporting Information Figure S5.
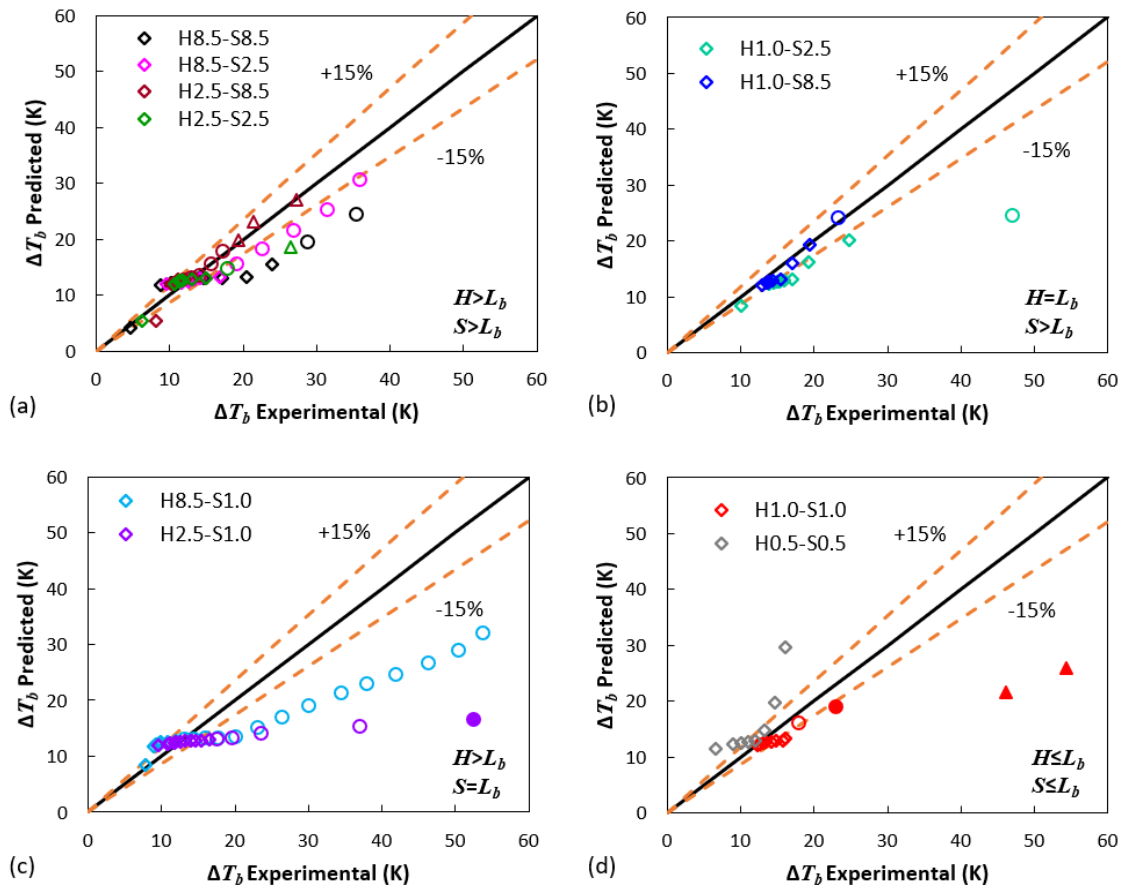

Figure 8: Predicted versus experimental superheats in HFE-7100. Heat sinks (a) with both height and spacing larger than L_b, (b) with height at L_b and spacing larger than L_b, (c) with height larger than L_b and spacing at L_b, and (d) with both height and spacing at or below L_b.

A comparison of the predictions and experimental data for boiling of heat sinks in water, shown in Fig. 9, yields the same takeaway as the HFE-7100 data. Namely, confinement effects cause a mismatch between the predictions and experimental data when the spacing is reduced below the capillary length. The predictions are accurate with both fin height and spacing above L_b, as shown in Fig. 9(a), as well as when height is reduced to the capillary length with a large spacing maintained, shown in Fig. 9(b). It should be noted that while the predictions and data do diverge at the highest superheats for both these subplots, this is for filled symbols that indicate the boiling was not stable. For samples with spacing at or below L_b, shown in Fig. 9(c) and (d), there is clear evidence of confinement effects causing a mismatch between the experiments and predictions. In particular, for 1.0 mm spacing, the data are significantly over predicted at lower superheats, indicating that the flat surface $h(\Delta T_b)$ cannot be applied to the fins. For 2.5 mm spacing, the effect is less pronounced but there is still evidence of confinement. Sample H2.5-S2.5 has excellent prediction agreement, but when the height is increased to 8.5 mm for the same spacing, the predictions increasingly diverge at high superheats, indicating that there is fin interference with the vapor due to inadequate spacing.
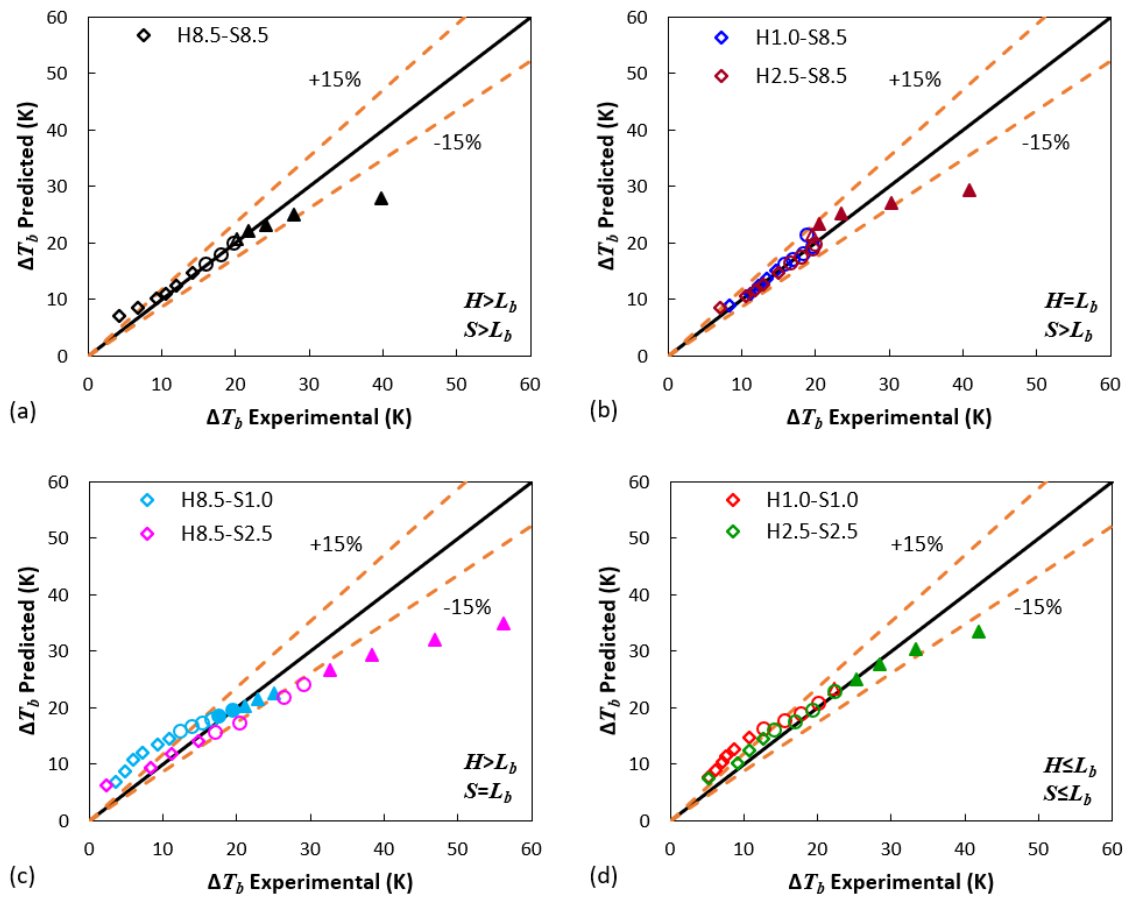

Fig. 9: Predicted versus experimental superheats in water. Heat sinks (a) with both height and spacing larger than L_b , (b) with height at L_b and spacing larger than L_b , (c) with height larger than L_b and spacing at L_b , and (d) with both height and spacing at or below L_b.

B. Critical Heat Flux

All samples that reached critical heat flux are compared to their predicted CHF values in Table 3. Focusing on HFE-7100, for the group of tallest fin heights H8.5-S8.5 and H8.5-S2.5, the CHF is increasingly underpredicted as spacing decreases. Recall these tallest samples had superheat predictions that were off by some constant, as indicated in Fig. 8(a), which is speculated to be the reason for this underprediction in CHF. Conversely, for samples with a height of 2.5 mm or 1.0 mm, the CHF is increasingly overpredicted as

spacing decreases. For the shortest 1.0 mm tall fins, the overprediction seems to stem from the fact that the shortest fins cannot sustain nucleate boiling from the fins while the base is covered with a vapor film. The experimental CHF values occur at nearly the same heat flux as the flat surface (23 W/cm^2), but the model erroneously predicts a range of heat flux operation where a vapor film boiling is sustained over the base, contrary to the experimental visualizations. For the case when both height and spacing were below L_b, H0.5-S0.5, the CHF value was significantly underpredicted. While this is different from other cases where fin height below L_b was unable to sustain boiling to predicted levels, the extremely small dimensions likely cause different boiling enhancement, such as increased nucleation site density and wicking effects.

Table 3: Predicted and experimental CHF values. Only samples that were stopped due to CHF are shown.

HFE-7100			
Sample (Height-Spacing)	**Experimental CHF (W/cm^2)**	**Predicted CHF (W/cm^2)**	**% Difference**
H8.5-S8.5	61.6	52.6	-14.6
H8.5-S2.5	101.0	72.7	-28.0
H2.5-S8.5	34.4	35.3	+2.6
H2.5-S2.5	35.5	43.7	+23.1
H2.5-S1.0	42.9	64.8	+51.0
H1.0-S8.5	24.7	26.1	+5.7
H1.0-S2.5	24.9	28.5	+14.5
H1.0-S1.0	28.9	34.4	+19.0
H0.5-S0.5	32.0	23.2	-27.5
Water			
Sample (Height-Spacing)	**Experimental CHF (W/cm^2)**	**Predicted CHF (W/cm^2)**	**% Difference**
H1.0-S8.5	142.8	298.5	+109.1
H1.0-S1.0	194.4	396.8	+104.2

For water, only two heat sink samples reached CHF in the experiments before the superheat limit was reached, both with a fin height 1.0 mm, significantly below the capillary length of 2.5 mm. Both have vastly over predicted CHF values. In the experiments the fins are enveloped in vapor at a heat flux slightly above CHF for the flat surface, with H1.0-S8.5 showing less than a 10% increase in CHF from the flat surface. This behavior that is not captured by the model predictions, as was the case for the 1.0 mm fins in HFE-7100. In summary, while the fin spacing with respect to the capillary length determined whether the superheat predictions held accurate, the fin height is the critical parameter that determined CHF. For a heat sink to provide enhancement of CHF above the flat surface by allowing nucleate boiling from the fin sidewalls after the base has a vapor film, the fin high must be larger than the capillary length L_b of the working fluid.

VI. CONCLUSIONS

It is confirmed the capillary length scale L_b offers a critical threshold for both the fin height and array spacing that determines the nature of boiling, as summarized in Fig. 10. For accurate prediction of the heat sink base superheat, the fin spacing (S) with respect to the capillary length is the dominant dimension that dictates whether fins can be assumed to boil independently following the

nucleate boiling behavior of a flat surface. When the spacing is above L_b, predictions incorporating the heat transfer coefficient $h(\Delta T_b)$ from a flat surface in the fin analysis hold accurate. However, when spacing is below L_b, the boiling curves exhibit a strong dependence on the spacing and experimental data diverge from predictions that assume isolated fins. Flow visualizations confirm there is confinement of vapor between the fins spaced below 1.0 mm for HFE-7100 and 2.5 mm for water, the respective capillary length scales of both fluids. The fin height (H) with respect to the capillary length determines whether the heat sink can extend CHF above that of a flat surface by allowing nucleate boiling to occur from the fins even after the base area has transition to film boiling. It is clear that fins must be longer than L_b to support a stable film at the base. Otherwise, the vapor will simply envelope the fins when a film forms over the base surface, leading to a CHF nearly the same as the flat surface.

Another key inference of the current work is that because the $h(\Delta T_b)$ boiling performance taken from a flat surface to accurately predict boiling on the vertical fin sidewalls, there is strong evidence that the orientation of the fins (horizontal versus vertical) does not have a significant effect for the geometries tested. The fact that the flat surface boiling performance can be used to predict boiling from fin arrays is of key importance to heat sink design for two-phase immersion cooling. This study defines a general criterion for the fin height and array spacing dimensions (larger than L_b), at which the prevailing modeling approaches can be applied to optimize simple finned heat sinks for boiling. The results also clearly identify the need for future work to expand these prediction capabilities to consider confinement effects and a wider range of optimized boiling heat sinks.
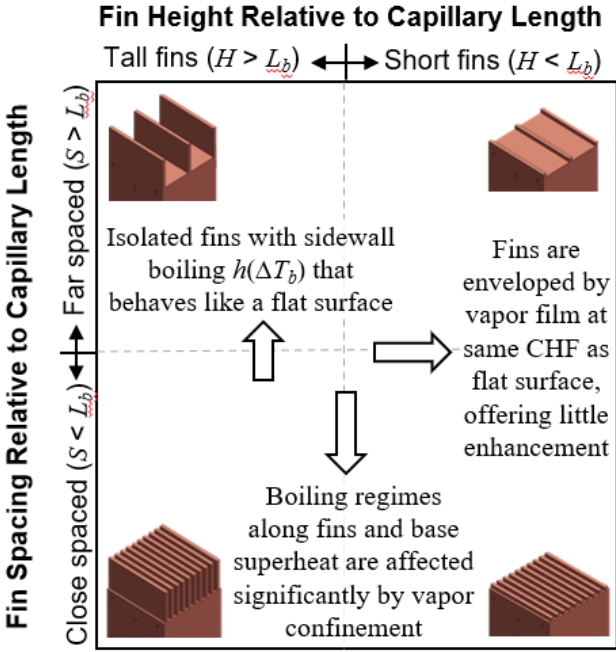

Fig. 10: Overall conclusions from both fluids. Samples with both fin height and spacing larger than L_b have accurate predictions, while fin height or array spacing less than L_b leads to incomplete predictions.

REFERENCES

[1] X. Yuan, X. Zhou, Y. Pan, R. Kosonen, H. Cai, Y. Gao, and Y. Wang., "Phase change cooling in data centers: A review," *Energy Build.*, vol. 236, p. 110764, 2021.

[2] X. Gong, Z. Zhang, S. Gan, B. Niu, L. Yang, H. Xu, and M. Gao, "A review on evaluation metrics of thermal performance in data centers," *Build. Environ.*, vol. 177, p. 106907, 2020.

[3] U. Sajjad, A. Sadeghianjahromi, H. M. Ali, and C.-C. Wang, "Enhanced pool boiling of dielectric and highly wetting liquids – A review on surface engineering," *Appl. Therm. Eng.*, vol. 195, p. 117074, 2021.

[4] G. Liang and I. Mudawar, "Review of pool boiling enhancement by surface modification," *Int. J. Heat Mass Transf.*, vol. 128, pp. 892–933, 2019.

[5] W. Li, R. Dai, M. Zeng, and Q. Wang, "Review of two types of surface modification on pool boiling enhancement: Passive and active," *Renew. Sustain. Energy Rev.*, vol. 130, p. 109926, 2020.

[6] B. J. Jones, J. P. McHale, and S. V. Garimella, "The influence of surface roughness on nucleate pool boiling heat transfer," *J. Heat Transf.*, vol. 131, no. 12, p. 121009, 2009.

[7] M.-G. Kang, "Effect of surface roughness on pool boiling heat transfer," *Int. J. Heat Mass Transf.*, vol. 43, no. 22, pp. 4073–4085, Nov. 2000.

[8] K. N. Rainey and S. M. You, "Pool boiling heat transfer from plain and microporous, square pin-finned surfaces in saturated FC-72," *J. Heat Transf.*, vol. 122, no. 3, pp. 509–516, 2000.

[9] S. Sarangi, J. A. Weibel, and S. V. Garimella, "Quantitative evaluation of the dependence of pool boiling heat transfer enhancement on sintered particle coating characteristics," *J. Heat Transf.*, vol. 139, no. 2, p. 021502, 2016.

[10] S. G. Liter and M. Kaviany, "Pool-boiling CHF enhancement by modulated porous-layer coating: theory and experiment," *Int. J. Heat Mass Transf.*, vol. 44, no. 22, pp. 4287–4311, 2001.

[11] G. Liang and I. Mudawar, "Review of nanoscale boiling enhancement techniques and proposed systematic testing strategy to ensure cooling reliability and repeatability," *Appl. Therm. Eng.*, vol. 184, p. 115982, 2021.

[12] S. Bhavnani, V. Narayanan, W. Qu, M. Jensen, S. Kandlikar, J. Kim, and J. Thome, "Boiling augmentation with micro/nanostructured surfaces: Current status and research outlook," *Nanoscale Microscale Thermophys. Eng.*, vol. 18, no. 3, pp. 197–222, 2014.

[13] C. M. Kruse, T. Anderson, C. Wilson, C. Zuhlke, D. Alexander, G. Gogos, and S. Ndao, "Enhanced pool-boiling heat transfer and critical heat flux on femtosecond laser processed stainless steel surfaces," *Int. J. Heat Mass Transf.*, vol. 82, pp. 109–116, 2015.

[14] T. P. Allred, J. A. Weibel, and S. V. Garimella, "Enabling highly effective boiling from superhydrophobic surfaces," *Phys. Rev. Lett.*, vol. 120, no. 17, p. 174501, 2018.

[15] K. Ferjančič, M. Može, P. Križan, M. Bobič, and I. Golobič, "Subcooled critical heat flux on laser-textured stainless-steel ribbon heaters in pool boiling of FC-72," *Int. J. Heat Mass Transf.*, vol. 159, p. 120090, 2020.

[16] A. R. Motezakker, A. K. Sadaghiani, S. Çelik, T. Larsen, L. G. Villanueva, and A. Koşar, "Optimum ratio of hydrophobic to hydrophilic areas of biphilic surfaces in thermal fluid systems involving boiling," *Int. J. Heat Mass Transf.*, vol. 135, pp. 164–174, 2019.

[17] T. P. Allred, J. A. Weibel, and S. V. Garimella, "The petal effect of parahydrophobic surfaces offers low receding contact angles that promote effective boiling," *Int. J. Heat Mass Transf.*, vol. 135, pp. 403–412, 2019.

[18] N. Abuaf, S. H. Black, and F. W. Staub, "Pool boiling performance of finned surfaces in R-113," *Int. J. Heat Fluid Flow*, vol. 6, no. 1, pp. 23–30, 1985.

[19] F.-S. Lai and Y.-Y. Hsu, "Temperature distribution in a fin partially cooled by nucleate boiling," *AIChE J.*, vol. 13, no. 4, pp. 817–821, 1967.

[20] D. R. Cash, G. J. Klein, and J. W. Westwater, "Approximate optimum fin design for boiling heat transfer," *J. Heat Transf.*, vol. 93, no. 1, pp. 19–23, 1971.

[21] C. Beurtheret, "L'ébullition à flux imposé sur paroi non isotherme," *Journ. Hydraul.*, vol. 7, no. 1, pp. 118–126, 1963.

[22] K. W. Haley and J. W. Westwater, "Boiling heat transfer from single fins," in *The 3rd International Heat Transfer Conference (IHTC)*, 1966.

[23] I. Mudawar and T. M. Anderson, "Optimization of enhanced surfaces for high flux chip cooling by pool boiling," *J. Electron. Packag.*, vol. 115, no. 1, pp. 89–100, 1993.

[24] G. Guglielmini, M. Misale, and C. Schenone, "Experiments on pool boiling of a dielectric fluid on extended surfaces," *Int. Commun. Heat Mass Transf.*, vol. 23, no. 4, pp. 451–462, 1996.

[25] F. Fantozzi, A. Franco, and E. M. Latrofa, "Analysis of the heat dissipation enhancement with finned surfaces in pool boiling of dielectric fluid," *Heat Mass Transf.*, vol. 36, no. 6, pp. 487–495, 2000.

[26] C. K. Yu and D. C. Lu, "Pool boiling heat transfer on horizontal rectangular fin array in saturated FC-72," *Int. J. Heat Mass Transf.*, vol. 50, no. 17–18, pp. 3624–3637, 2007.

[27] G. J. Klein and J. W. Westwater, "Heat transfer from multiple spines to boiling liquids," *AIChE J.*, vol. 17, no. 5, pp. 1050–1056,1971.

[28] W. R. McGillis, V. P. Carey, J. S. Fitch, and W. R. Hamburgen, "Pool boiling enhancement techniques for water at low pressure," in *The 7th IEEE Semiconductor Thermal Measurement and Management Symposium*, pp. 64–72 1991.

[29] I. Mudawar and T. M. Anderson, "Parametric investigation into the effects of pressure, subcooling, surface augmentation and choice of coolant on pool boiling in the design of cooling systems for high-power-density electronic chips," *J. Electron. Packag.*, vol. 112, no. 4, pp. 375–382, 1990.

[30] T. Harirchian and S. V. Garimella, "A comprehensive flow regime map for microchannel flow boiling with quantitative transition criteria," *Int. J. Heat Mass Transf.*, vol. 53, no. 13, pp. 2694–2702, 2010.

[31] M. J. Rau and S. V. Garimella, "Local two-phase heat transfer from arrays of confined and submerged impinging jets," *Int. J. Heat Mass Transf.*, vol. 67, pp. 487–498, 2013.

[32] C. Mira-Hernández, J. A. Weibel, and S. V. Garimella, "Visualizing near-wall two-phase flow morphology during confined and submerged jet impingement boiling to the point of critical heat flux," *Int. J. Heat Mass Transf.*, vol. 142, p. 118407, 2019.

[33] M. D. Clark, J. A. Weibel, and S. V. Garimella, "Identification of nucleate boiling as the dominant heat transfer mechanism during confined two-phase jet impingement," *Int. J. Heat Mass Transf.*, vol. 128, pp. 1095–1101, 2019.

[34] M. J. Rau and S. V. Garimella, "Confined jet impingement with boiling on a variety of enhanced surfaces," *J. Heat Transf.*, vol. 136, no. 10, p. 101503, 2014.

[35] K. Brown, H. Coleman, and W. Steele, "Estimating uncertainty intervals for linear regression," in *The 33rd Aerospace Sciences Meeting and Exhibit*, 1995.

[36] J. R. Lloyd and W. R. Moran, "Natural convection adjacent to horizontal surface of various planforms," *J. Heat Transf.*, vol. 96, no. 4, pp. 443–447, 1974.

[37] N. Zuber, "On the stability of boiling heat transfer," *Trans. Am. Soc. Mech. Eng.*, vol. 80, no. 3, pp. 711–714, 1958.

[38] P. J. Berenson, "Film-boiling heat transfer from a horizontal surface," *J. Heat Transf.*, vol. 83, no. 3, pp. 351–356, 1961.